ACS Biomaterials SCIENCE & ENGINEERING
Cite This: ACS Biomater. Sci. Eng. 2019, 5, 5916−5924
Article
pubs.acs.org/journal/abseba

Deformation Mechanisms of "Two-Part" Natural Adhesive in Bone Interfibrillar Nano-Interfaces

Reza Morsali,[†] Zhengwei Dai,[‡] Yang Wang,[†] Dong Qian,[†] and Majid Minary-Jolandan*[,†]

[†]Department of Mechanical Engineering, The University of Texas at Dallas, 800 W. Campbell Rd, Richardson, Texas 75080, United States

[‡]College of Material and Textile Engineering, Jiaxing University, Jiaxing 314001, China

Supporting Information

ABSTRACT: Noncollagenous proteins at nanoscale interfaces in bone are less than 2−3% of bone content by weight, while they contribute more than 30% to fracture toughness. Major gaps in quantitative understanding of noncollagenous proteins' role in the interfibrillar interfaces, largely because of the limitation of probing their nanoscale dimension, have resulted in ongoing controversies and several outstanding hypotheses on their role and function, arguably going back to centuries ago to the original work from Galileo. Our results from the first detailed computational model of the nano-interface in the bone reveal "synergistic" deformation mechanism of a "double-part" natural glue, that is, noncollagenous osteopontin and osteocalcin at the interfibrillar interface. Specifically, through strong anchoring and formation of dynamic binding sites on mineral nanoplatelets, the nano-interface can sustain a large nonlinear deformation with ductility approaching 5000%. This large deformation results in an outstanding specific energy to failure exceeding ∼350 J/g, which is larger than the most known tough materials (such as Kevlar, spider silk, and so forth.).

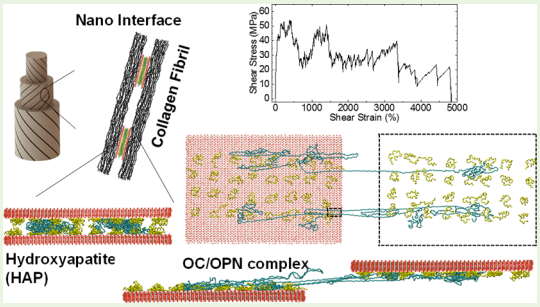

KEYWORDS: *bone protein interface, bone toughness, nano-interface, natural glue, steered molecular dynamics, energy dissipation, computational simulation*

The fracture toughness of the cortical bone is remarkable (∼10−100 kJ m^{-2}), while the bone is also simultaneously stiff and strong [specific modulus of up to ∼20 GPa/(Mg m^{-3}), and specific strength of up to ∼30 MPa/(Mg m^{-3})]. The stiffness and strength of bone can be largely explained by ∼60% hydroxyapatite (HAP) nanomineral content in the bone nanocomposite structure. However, the origin of fracture toughness in bone is more complex. Bone cracks, however, it does not easily fracture under propagation of existing cracks. In other words, bone has "intrinsic" energy dissipation mechanisms that make it more difficult for a crack to propagate than to initiate.[1−6]

For enhanced fracture toughness, a material should be able to dissipate energy from mechanical loads to limit crack formation, and hence, intrinsic energy dissipation mechanisms become important. Additionally, the material should be able to redistribute stresses around the existing cracks and defects, which results in the reduction of the crack tip sharpness and stress concentration. To achieve damage tolerance, energy for crack opening should increase as the crack size increases, such that the cracks are contained and do not propagate. Often times, the constituents of a composite do not exhibit these properties, and therefore, the interfaces between the hard−soft constituents should provide these characteristics and exhibit inelastic deformation with large toughness (energy under stress−strain response). Additionally, although macroscale deformation can be small, the interface should exhibit large deformation at the microscale and maintain cohesion for deformation of possibly many times of the interface thickness. The interface should be strong enough to maintain the integrity of the composite, while it should be considerably weaker than the other constituents of the composite to be able to transfer deformation. In composites including bone, the main function of interfaces is the mechanical load transfer across length scales between building blocks. As such, they play a critical role in the deformation mechanisms of the composite as well.[4]

Bone has two main interfaces, namely, the "interfibrillar interfaces" and "cement lines". The cement line (1−5 μm in thickness) is the interface between the osteons and the surrounding interstitial bone. The cement lines contribute to bone toughness through crack deflection and twist in the transverse (to the cement line) orientation and crack bridging (the formation of uncracked ligament bridges) in the longitudinal (splitting) orientation. The cement lines are the reason that it is approximately five times more difficult to break the bone than to split it. In bone, although the major crack deflection and bridging occur at the microscale, however, the

Received: April 29, 2019
Accepted: September 24, 2019
Published: September 25, 2019

DOI: 10.1021/acsbiomaterials.9b00588
ACS Biomater. Sci. Eng. 2019, 5, 5916−5924

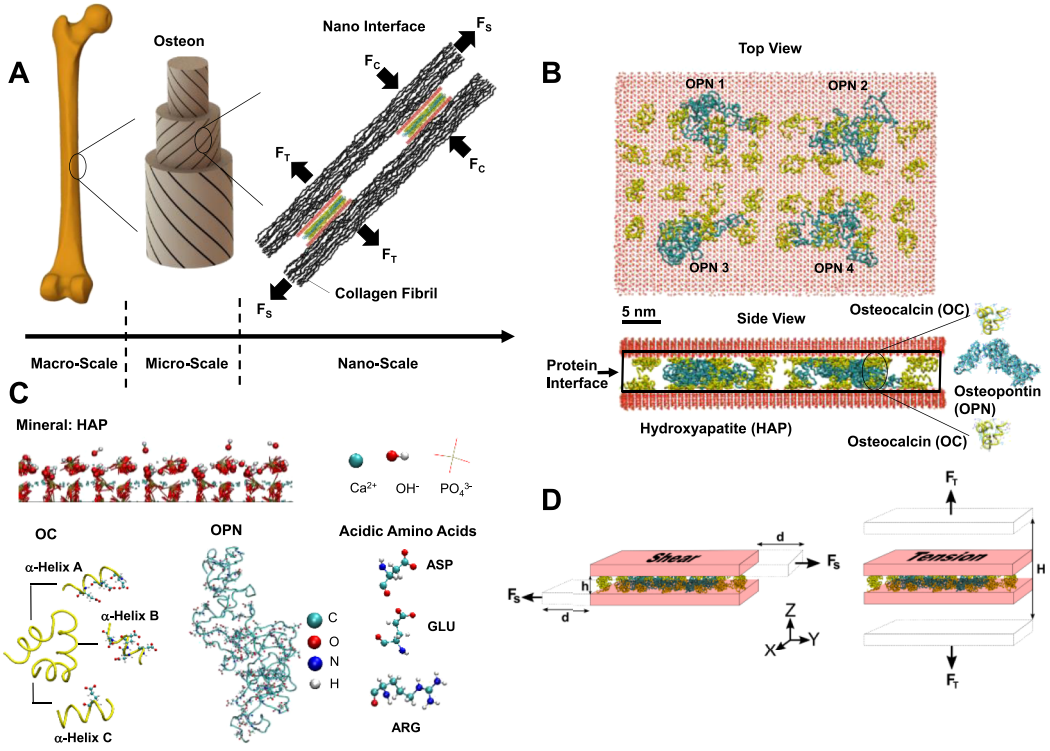

Figure 1. (A) Hierarchical structure of cortical bone and the nano-interface between two collagen fibrils. (B) Configuration of the nano-interface (OPN and OC chains are colored blue and yellow, respectively). The nano-interface is a 3-layer structure of two biopolymers sandwiched between two HAP platelets. Two layers of OC molecules are anchored onto the HAP platelets and one layer of OPN molecules is between two OC layers. The thickness of the nano-interface is 7.4 nm, including the thickness of the mineral platelets. The rectangle shows the overall shape of the interface in the initial state. (C) Structure of OC, OPN chains, and HAP platelets. The atomistic structure of the ASP, GLU, and ARG residues, which play an important function in the deformation and mechanics of the biopolymers at the interface. HAP is plotted as the ball and stick model. (D) Simplified structure of the nano-interface under shear and tension deformation.

ductility originates from the nanoscale.[7,8] The interfibrillar interface is the interface between individual collagen fibrils within the bundle that forms collagen fibers (Figure 1A). These interfaces are a few nanometers (~2.6 nm) in thickness. The interface is filled with noncollagenous proteins, mainly osteopontin (OPN) and osteocalcin (OC). These proteins can be considered as "natural glue", given their adhesive function at the interface.[9] In bone, individual collagen fibrils are mineralized. The mineral (HAP) nanocrystals are embedded inside collagen fibrils and also cover the surface of the fibrils. Hence, noncollagenous proteins (OPN and OC) essentially form a sandwich structure with mineral platelets at the interface (Figure 1B).[4]

Interfaces constitute only up to a few percent of a composite mass, however, they contribute up to several tens percent to the fracture toughness of the composite. For example, in enamel, the proteins comprise ~1% of the total enamel weight, while they are responsible for ~40% of total fracture toughness. Another example is bone. By weight, approximately 60% of bone is composed of mineral (calcium and phosphate, in the form of HAP), 10−20% water, and 20−30% proteins. About 90% of the protein content is type I collagen, and the remaining 10% is non-collagenous proteins, including fibronectin, osteonectin, sialoprotein, OC, and OPN. OPN is believed to be the most abundant noncollagenous protein in bone. Therefore, the interfibrillar interface proteins are less than 2−3% of bone content by weight, while they contribute to more than 30% of fracture toughness.[10]

"Sacrificial bonds" have been hypothesized as one of the energy dissipation mechanisms in bone. It has been suggested that the calcium-mediated sacrificial bonds in the bone could form between two binding regions on one or both of the interface proteins, and/or between an interface protein and a mineral platelet or a combination of these. Additionally, each sacrificial bond might have multiple weak bonds in parallel. In vitro study has shown that recombinant OPN forms networks (stabilized with sacrificial bonds) that can dissipate a large amount of energy through working against the entropy by breaking sacrificial bonds and (mainly) by the stretching of the hidden length. It was also observed that energy dissipation significantly increased with the addition of Ca^{2+} ions. The atomic force microscope pulling experiment on this OPN network showed an average pulling length over 1 μm. This length corresponds to the length of more than 10 OPN macromonomers aligned end-to-end in one chain. The average maximum pulling force was on the order of 1 nN, with estimated ~100 pN sacrificial bond strength.[11−15]

Recently, evidences for "dilatational bands" formation in bone at the nanoscale were reported, suggesting that the fracture initiation occurs in the bone at the nanometer scale by these bands.[16] Dilatational bands were defined as the ellipsoidal voids of the order of 100 nm formed as a result of noncollagenous protein complexes deformation between fused mineral aggregates. It was argued that dilatational band formation is crucial for bone toughness. Staining analysis showed that OC and OPN colocalize within dilatational bands. It was suggested that the absence of either protein at the

DOI: 10.1021/acsbiomaterials.9b00588
ACS Biomater. Sci. Eng. 2019, 5, 5916−5924

interface resulted in dramatic loss of bone toughness. The total extension of the OC/OPN complex was estimated to be ~135 nm. The role of OC and OPN proteins in regulating the dilatational band formation was confirmed by fracture experiments on bones from knockout animal models. Specifically, bone lacking in OC, OPN, or both showed dramatic (~80%) reduction in diffused damage and significant (~30%) reduction in fracture toughness. When the protein complexes at the interface rupture, two adjacent collagen fibrils slide with respect to each other or separate depending on the type of the external load, which ultimately results in formation of diffused damage regions, which may be followed by linear microcrack formation.

Despite significant roles of interfibrillar interfaces, current knowledge of their structural organization, deformation mechanisms, and the role of each protein is very limited. In this study and for the first time, we present the detailed deformation mechanisms of the proteins in the bone interfibrillar interfaces. Our results from the detailed computational model of the nano-interface reveal "synergistic" deformation mechanisms of a "two-part" natural glue (i.e., noncollagenous OPN and OC) at the interfibrillar interface. Specifically, through strong anchoring and formation of dynamic binding sites on mineral nano-platelets, the nano-interface can sustain a large nonlinear deformation with ductility approaching 5000%. This large deformation results in an outstanding specific energy to failure exceeding ~350 J/g, which is larger than the most known tough materials (such as Kevlar, spider silk, and so forth.).

RESULTS AND DISCUSSION

In bone under tension, the overall tension is accommodated by shearing of the interfibrillar interfaces, which is often referred to as nanoscale ductility responsible for significant energy dissipation[17] and the tension of the mineralized fibrils.[18,19] During bone fracture, individual fibrils and/or the bundles of fibrils (fibers) are pulled out of the crack faces and are either ruptured or form bridges within the crack.[20−23] Interface proteins are deformed during this pull-out process.[24,25] In the load-bearing cortical bones (such as femur), the fibrils are in helical geometry (3-dimensional),[18,26] as shown in Figure 1A, therefore, under tension or compression, the proteins in the interface are under combined tension/compression and shear deformation. The stress−strain responses of the nano-interface under shear and tensile deformation are shown in Figure 2A,B, respectively. The specific energy to failure represents the maximum energy a material can absorb before failure, normalized by the mass of the nano-interface. The specific energy was obtained from the area under each stress−strain response up to the failure point (Figure 2A,B). We observed that the interface sustains remarkable strain values of ~4835 and ~2419% under shear and tension, respectively. In particular, under shear loading, the nano-interface exhibits a combination of strain softening and strain hardening, which combined with the large ductility results in an outstanding specific energy to failure exceeding ~350 J/g. This specific energy is several times larger than the specific energy of most commonly known tough materials, such as the spider silk, Kevlar, and carbon nanotube yarns (Figure 2C).[27−38]

The nano-interface under tension shows a large sudden drop in stress after the yield point ~14% strain and continues to stretch at a stress level of 10−20% of the peak stress up to the failure point of ~2419%. The specific energy to failure under

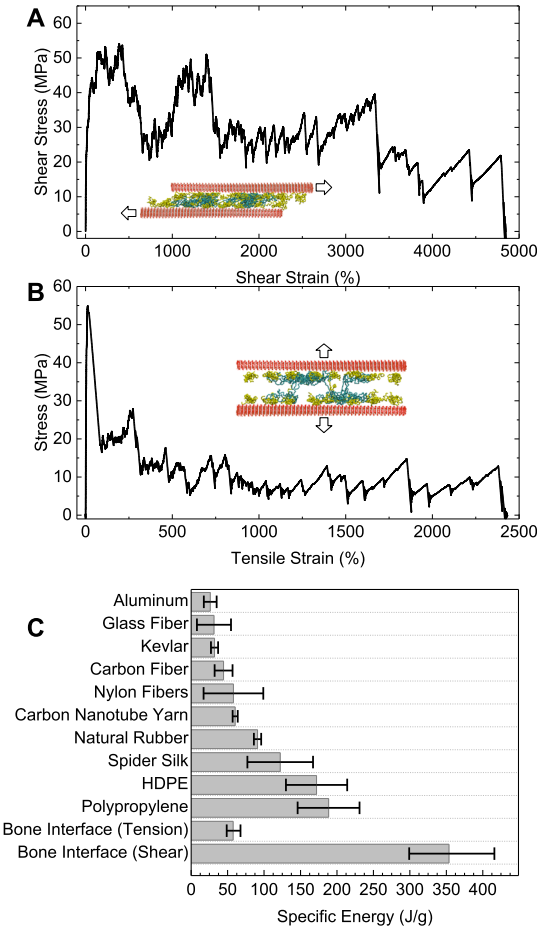

Figure 2. (A,B) Stress−strain responses of the nano-interface under shear and tension deformations, respectively. The total simulation time for shear and tension was 62.6 and 34.2 ns, respectively. (C) Comparison of specific energy to failure (specific toughness) with other tough materials.[27−38] The specific energy of the nano-interface under shear deformation is ~six times higher than tension.

tension reaches ~58 J/g. Although this value is six times smaller than shear loading, it is still remarkable compared to other tough materials (Figure 2C). Interface behavior under compression is shown in Figure S1. Under compression, strain increases to the value of 75%, which is much smaller than the strain under shear and tension. The specific energy to failure under compression is calculated to be 61.7 J/g.

Other detailed mechanical properties under shear and tension deformation are provided in Figure S2. Given the remarkable energy dissipation capability of the interfibrillar interface, we aimed to understand the origin of such outstanding properties, as well the molecular mechanisms of the cooperative deformation at the interface, and the role of OPN and OC in the mechanics of the interface under shear and tensile deformations.

The initial configuration corresponding to zero strain is shown in Figure 1B. Figure 3 shows the snapshots of the molecular dynamics (MD) simulation during the shear deformation of the interface. Overall, during deformation, OC chains are tightly bound to the HAP surface, while OPNs initially get sheared and then gradually start peeling off from OCs and roll on the adjacent OCs in the shear direction (Figure 3A,B). Additionally, OPN chains penetrate through OCs to reach the HAP surface and form new OPN/HAP

DOI: 10.1021/acsbiomaterials.9b00588
ACS Biomater. Sci. Eng. 2019, 5, 5916−5924

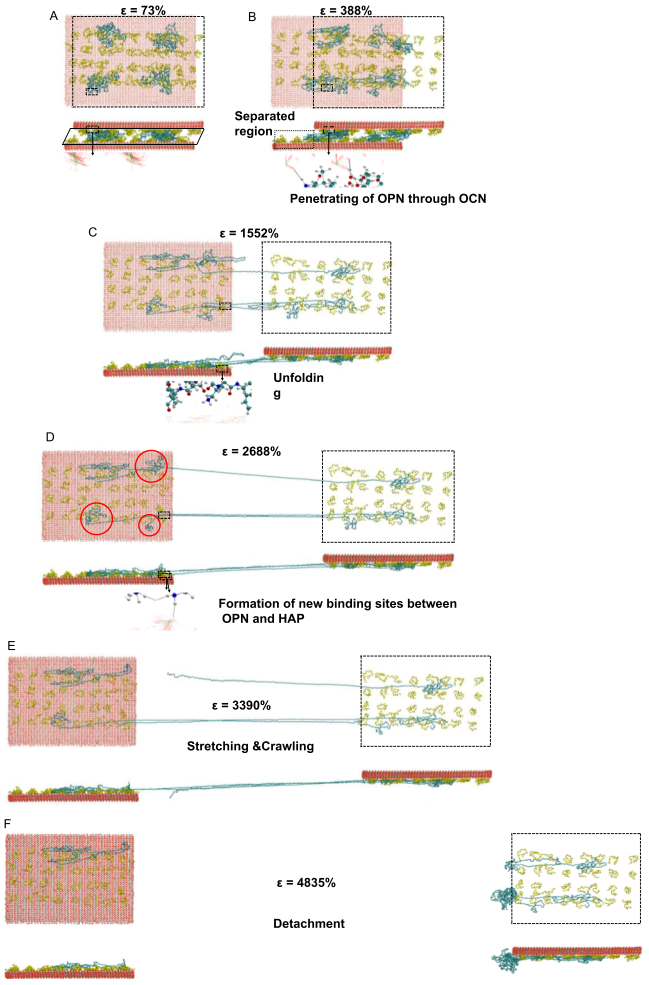

Figure 3. Snapshots of the interface at different shear strains show the configuration and interaction between interface constituents (corresponding to the red points in Figure 4A). The dashed rectangle demonstrates top HAP. Water and calcium (Ca^{2+}) ions are removed for clarity. (A) Deformed configuration in the elastic region at ∼73% shear strain. The nano-interface is stretched in the shear direction and the rectangle in initial configuration (Figure 1B) is deformed into a parallelogram. (B) Yield point at ∼388% shear strain. Eight OCs at the top and 8 OCs at the bottom layer are fully detached from each other. Dashed rectangle shows the separated region of the interface. The dashed line in the inset shows the hydrogen bonds formed between OPN and HAP. (C) The strain softening region at ∼1552% shear strain. All OC/OC bonds between the OCs on top and bottom platelets are broken. (D) Strain softening with the constant stress region at the strain of ∼2688%. Red circles show the ends of OPNs where unfolding happens. (E) Strain hardening region at the shear strain of ∼3390%. The detachment of OPN 3 from the bottom HAP causes a sudden drop in the stress−strain graph (Figure 4A). (F) Snapshot of the failure at the strain of ∼4835% (the total simulation is was 62.6 ns).

binding regions (Figure 3B inset). Bindings between OPN/OC and OPN/HAP breaks and reforms ("dynamic binding sites") as OPNs roll and slide in the shear direction, which results in the dissipation of a large amount of energy. Under larger strain, the binding sites of OPN/OC and OPN/HAP tightly hold two ends of the OPN on the HAP surface, and hence allow OPN chains to unravel and stretch without detaching from HAP. This "anchoring" of OPN on HAP, mostly provided by OC, is strong such that the unfolding and detaching of OPN from HAP starts from one side of OPN that has less binding sites with OCs and other OPNs (red circles in Figure 3D).

Deformation mechanisms of the interface can be explained quantitatively in terms of changes in the configuration (shape) of the proteins and the number and energy of noncovalent interactions between the different constituents of the interface, that is, OPN, OC, and HAP. In particular, for configuration change, we consider changes in the bond energy, that is, bond stretch energy, bond angle energy, dihedral energy (Figure 4C), and the gyration radius (Figure 4D,E) of the protein

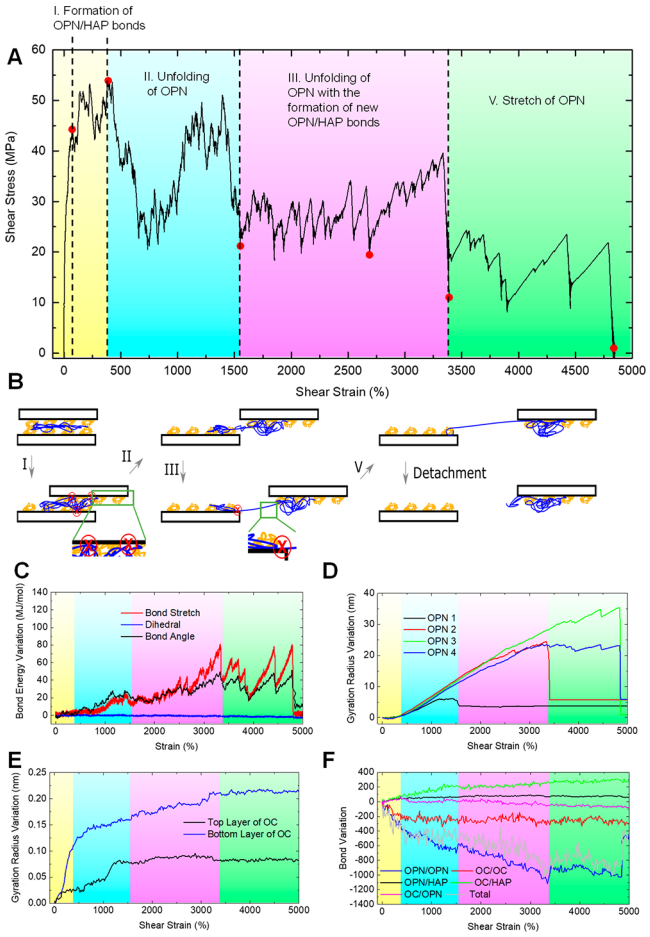

Figure 4. (A) Strain−stress response of OC/OPN nano-interface in bone under shearing. Color-coded regions are as follows: elastic and yielding (yellow), strain softening and stress drop (blue), strain softening with almost constant stress (purple), and strain hardening (green). Red dots are the selected points at which interface configuration is shown in Figure 3. (B) Schematic figure shows the different stages of the interface deformation mechanisms under shear. (C) Corresponding change in bond energies, that is, bond stretch, bond angle, and dihedral energies vs strain. (D,E) are the corresponding changes in the gyration radius of 4 OPNs and OC layers vs strain, respectively. (F) Plot shows variations of the nonbonded interactions vs strain.

chains. The interaction energy (Figure S3) includes electrostatic and van der Waals interactions, with a negative value indicating attractive interaction. The variation in the number of bonds between proteins and HAP are depicted in Figure 4F. We note that changes in interaction may lead to the configuration changes. For instance, constant interaction between proteins and HAP leads to continuous deformation

DOI: 10.1021/acsbiomaterials.9b00588
ACS Biomater. Sci. Eng. 2019, 5, 5916−5924

of the protein chains and bonds failure, which leads to detachment and sudden configurational change of the protein.

The stress−strain response under shear deformation includes four distinct phenomena (Figure 4A). These are highlighted in the stress−strain curve and represented schematically in Figure 4B, and include (i) the elastic deformation followed by the penetration of OPN through OC for dynamic bond formation between OPN/HAP, (ii) unfolding of OPN, (iii) unfolding of OPN and formation of new OPN/HAP binding sites, and (iv) stretching and crawling of OPN chains followed by chain failure. These phenomena result in mechanical yielding of the interface, strain softening, and strain hardening behavior observed in the stress−strain response. Within the strain softening range, stress dropped ∼61%, from ∼54 to 21 MPa, and then maintained at the stress level of ∼20−40 MPa afterward. There was another sudden drop in stress at the strain of ∼3390%, following which stress increased to ∼24 MPa (stress hardening). The failure occurs by several gradual drops in stress up to the final rupture point at the strain of ∼4835%.

Elastic Deformation Mechanism. Under shear deformation, the interface initially deforms elastically up to the strain of ∼73%. The elastic deformation is accommodated by the slight flattening and elongation of OCs over the surface of HAP platelets as indicated by the increase of their respective radius of gyration (Figure 4E). Additionally, within the elastic deformation region, the total number of OC/HAP bonds increases (Figure 4F), which shows that the number of OC/HAP bonds that form is more than the number of OC/HAP bonds that break. The results also show that within the elastic range, the number of OC/OC bonds decreases by ∼245 (Figure 4F). All three bond energy terms are almost constant within the elastic region. The change in the number of bonds is mainly responsible for the configurational change in the elastic region. Both OCs and OPNs contribute to the elastic deformation.

Yielding Mechanism. After the elastic strain of ∼73%, OPNs start penetrating through OCs to reach to the surface of HAP platelets. In addition, the top and bottom OC layers start to detach from each other. The number of OPN/HAP bonds increases by 52 at the end of the elastic region. The inset in Figure 3B shows a snapshot of this process. Additionally, OPNs start sliding and rolling on OC layers. These processes together result in the mechanical yielding of the interface. The interaction energy between OPN/HAP is ∼−27 and ∼−43 MJ/mol at zero strain and at the yield point, respectively (Figure S3B). In particular, three amino acids aspartic acid (ASP), glutamic acid (GLU), and arginine (ARG) in OPN were found in the binding sites with HAP (Figure S4). These binding sites are dynamic and break and reform along the surface of HAP platelets during deformation. These dynamics binding sites play important roles in carrying the force in subsequent large deformation in the nano-interface.

Strain Softening Region. After yielding, OPN chains experience large deformation. This large deformation is enabled by the anchoring of their ends on the surface of the HAP supported by OCs (Figures 3C,D, and S5). Initially, up to the strain of ∼1552%, this large deformation continuously changes the configuration of OPNs by unfolding the protein. As less force is required to unravel the remaining part of the protein, force eventually reduces, which shows up as strain softening with stress drop in the stress−strain diagram (Figure 4A). With further strain beyond ∼1552%, the OPN chains start aligning in the direction of shear. In the strain range of ∼1552 to ∼2688%, the strain is accommodated by the unfolding of the OPN chains. In this range of strain, OPN chains unfold while approaching and creating new dynamic binding sites with the HAP surface (Figure 3D inset). This combined unfolding and binding results in a relatively constant level of stress in this strain range.

Qualitatively, at the end of the strain softening region (∼3390%), the average R_g of OPNs increases by ∼20 nm from the initial configuration at zero strain. Initially, up to the strain of ∼1552%, increase in the bond stretch is smaller than the bond angle as the OPNs are being unfolded. In the strain range of ∼1552 to ∼3390%, the rate of increase in the bond stretch energy is larger than other bond energies because OPN chains are aligned in the shear direction and are being stretched. The bond variation of OPN/OPN shows 1120 breakage of the bonds at the end of the strain softening region, as the OPNs are being unfolded and stretched (Figures 3E and 4F). The number of bonds between OPN/HAP initially increases during the yielding process (as the OPN penetrates through OC to form bonds with HAP) and unfolding up to a strain value of ∼1552% (Figure 4F). Afterward, within the strain values of ∼1552 to ∼3390%, the number of bonds (Figure 4F) and interaction energy (Figure S3B) between OPN/HAP remains relatively constant, which support the fact that the number of bonds that break and reform are approximately the same as the OPN uncoils. The increase in the stretched length (free length) of the three active OPNs (OPN 2−4 in Figure 1B) during the softening region is shown in Figure S6.

Strain Hardening Region. For strain larger than ∼3390%, only two chains of OPNs (OPN 3 and 4) carry the force between two HAP platelets (Figure 3E). In this strain range, the only configuration change is the stretching of OPN chains. These OPN chains undergo large stretch in their backbone. The sudden jumps and drops in the stress, bond stretch energy, and bond angle energy correspond to sudden changes in the configuration of OPNs, their stretch and failure of different chains. The interaction energy of OPN/HAP is ∼−45.8 MJ/mol at a strain of 3390% and changes to ∼−41.8 MJ/mol at the failure point. This change in the energy level is due to detachment of the OPNs from HAP platelets.

OC and OPN Roles in the Deformation Mechanism. OPN is a long chain, which can directly connect two platelets through HAP/OPN interaction, while OC is a short chain (∼9.6 times shorter than OPN), which cannot directly transfer any load between the platelets, rather OCs transfer the load through other OCs and OPNs. OCs also function as anchors for OPNs (Figure S5) on the surface of HAP platelets. OCs move with HAPs because they firmly adhere to HAP throughout several binding sites shown in Figure S7. OPNs, however, move over the HAP surface and get anchored to OC chains as they move. The entanglement among OPNs and OCs enhances the load-transfer capacity of the interface because it improves attachment of OPNs to the HAP platelets. The number of bonds between OC/HAP monotonically increases during deformation (Figure 4F). Similarly, the absolute value of interaction energy between OC/HAP increases and slowly tapers off during deformation (Figure S3A). This behavior shows that each OC flattens over on the surface of HAP (Figure 4E), which enlarges their surface area with HAP. OCs form strong bonds with HAP and remain relatively stationary during deformation. Shearing deformation facilitates mostly A and B alpha helices of the OCs to find their

DOI: 10.1021/acsbiomaterials.9b00588
ACS Biomater. Sci. Eng. 2019, 5, 5916−5924

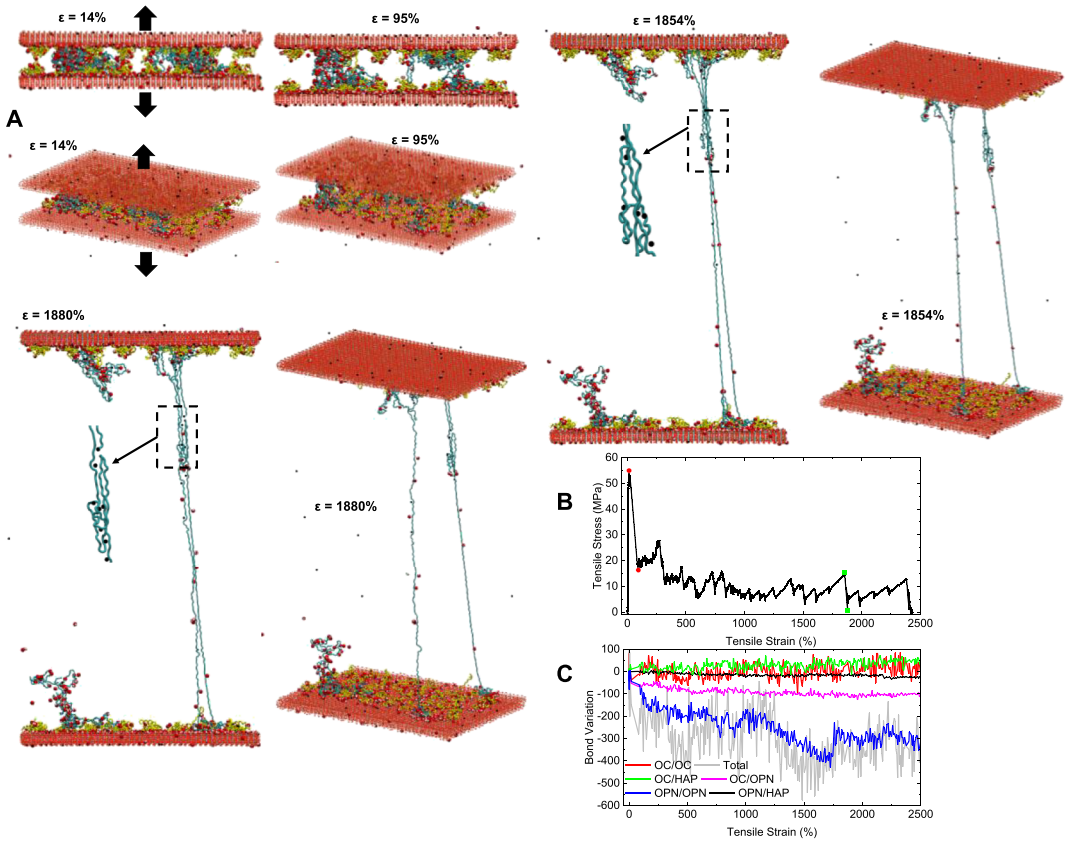

Figure 5. (A) Snapshots of nano-interface behavior under tensile deformation at different strains. Water molecule and calcium ions are depicted as red and black dots, respectively. The zoomed-in view shows dynamic bonds in the OPN chain mediated by calcium ions. (B) Stress−strain under tensile loading. Red and green dots are the selected points at which interface configuration is shown in (A). (C) Variations of bonds vs tensile strain.

way to the surface of HAP, which enhances OC/HAP attachment.

ASP and GLU residues on OCs form bonds with calcium Ca^{2+} ions on the HAP surface while ARG forms bonds with PO_4^{3-} and OH^- (Figure S7). As control models, we also developed different nano-interface models where OC or OPN was removed. Overall, the disruption of the complex due to the absence of either one resulted in poor linking between the mineral aggregates and a consequent inability to dissipate large energy. It was found that properties of the "double-protein" interface are superior to properties of each of its constituents.

Tensile Behavior of the Nano-Interface. The behavior of the nano-interface under tensile deformation is shown in Figure 5A. The stress−strain curve and variations in the number of bonds are also shown in Figure 5B,C, respectively. The main characteristic of the tensile behavior of the interface is the rapid increase in the stress within the elastic range, followed by a sudden drop in stress (red dots in Figure 5B). After the sudden drop in stress, the OPN chains are unfolded and stretched, which results in a large strain at a low stress level up to the failure point. During the sudden drop in stress, the number of bonds for OPN/OPN and OPN/OC interactions decreases.

Within the initial stage of tension, OPNs are indirectly connected to HAP platelets through OCs, while OCs are firmly attached to the HAP surface through ASP, ARG, and GLU residues (Figure S7). With further tension after the elastic range, the number of bonds between OPNs and OCs suddenly drops, as the interfaces "splits", which can be observed in Figure 5C from the variation of the bond number between OC/OC and OC/OPN. At this point, only OPNs maintain the connection between the two HAP platelets. The sudden split between OPNs and OCs between two platelets results in the sudden drop in stress.

The saw-tooth behavior of the stress after the yield point is due to changes in the interaction and configuration of OPNs. Dynamic bonds within OPN chains continuously break and reform throughout the process. These bonds are formed between the amino acid residues in protein chains (Figure S9) and between the amino acid residues and Ca^{2+} ions (Figure S10). The sudden drop in the stress−strain (Figure 5B) at the strain ∼1870% (green squares in Figure 5B) is due to the breakage and formation of dynamics bonds between OPN and Ca^{2+} ions (Figure 5A inset). During tension, the number of OPN/HAP bonds remains unchanged while the number of OPN/OC bonds varies (Figure 5C). Therefore, it can be concluded that OPNs are mainly connected to HAP through OCs. Similar to shear deformation, the OCs tightly anchor the ends of the OPNs on the HAP platelet surface, which forces the OPN chains to fully stretch up to the failure point, without detachment from the platelets (Figure 5A).

The variation in the gyration radius and bond energy of the protein chains are shown in Figure S8. The sudden drops in gyration radius variation of OPNs are due to the coiling back and detachment of OPN from top or bottom HAP (Figure S8E). At strain ∼945%, OPN 3 detaches from its anchorage point with OCs and HAP, which results in a decrease in stress. After failure, OPN chains coil back, which results in a sudden

DOI: 10.1021/acsbiomaterials.9b00588
ACS Biomater. Sci. Eng. 2019, 5, 5916−5924

jump in the bond variation of OPN/OPN (Figure 5C). In simulations, no restriction on HAP deformation was applied, and they were free to break or fracture during shear and tension. However, the minerals did not fail during shear and tension of the nano-interface because of strong electrostatic interactions between Ca^{2+}, OH^-, and PO^{3-}.[18]

In conclusion, our atomistic simulation reveals a unique synergistic deformation mechanism between the two proteins at the interfibrillar interface in bone. OCs were found to tightly anchor the ends of the OPNs on HAP mineral platelets, and hence force the bundled OPN chains to fully stretch between two platelets. Additionally, OPN chains were found to form dynamic binding sites on OC and even penetrate through the OC layer to bind to HAP during shear deformation. Together, these two proteins that constitute only ∼2−3% of bone weight function as a double-part glue and sustain a large nonlinear deformation with ductility approaching 5000%. This large deformation results in an outstanding specific energy to failure exceeding ∼350 J/g, which is larger than the most known tough materials (such as Kevlar, spider silk, and so forth.). Given their significant contribution, these interface proteins may also be important enough to be considered as one of the building blocks of bone. Diseases such as osteoporosis, and genotypes such as OPN deficiency may significantly compromise the composition and mechanics of the nano-interface and result in degradation of mechanical properties of bone, hence development of standard tests for assessing composition and quality of the interface in bone may be relevant.

MATERIALS AND METHODS

OPN, OC, and HAP Models. The configuration of OC was adopted from the protein data bank (pdb ID "1VZM")[39] and was formatted into an input file for the MD simulation package, GROMACS. OPN is an amorphous protein. The OPN residue sequence was adapted from the National Center for Biotechnology Information, the U.S. National Library of Medicine (ID D053495).[40] The model of the OPN chain was generated according to the residue sequence. Subsequently, each residue was positioned with random initial coordinates. The chain model was equilibrated at 300 K for 20 ns. After that, the OPN chain was submerged inside a water box of 25 × 25 × 25 nm^3 and equilibrated for another 10 ns. Subsequently, the OPN chain was extracted and formatted into a GROMACS input file.

The 3D structure of the HAP unit cell contains 44 atoms,[41] with lattice parameters of a = 9.417 Å, b = 9.417 Å, c = 6.875 Å, $\alpha = 90°$, $\beta = 90°$, and $\gamma = 120°$.[42] The [001] HAP surface was utilized in the models, on which Ca^{2+} ions and hydroxy cations were distributed. OPN chains have a rich content of ASP and GLU residues. These residues are negatively charged and tend to adhere to the HAP surface (Figure S4). The OC molecule is one chain composed of 3 alpha-helices, that is, A, B, and C (as shown in Figure 1C). Of the 3 alpha helices, A and B have the most abundant ARG and GLU residues, and therefore, OC tends to adhere to the HAP platelet surface through the alpha helices A and B (Figure S7). Each OC and OPN chain contain 493 and 4741 atoms, respectively. The negatively charged carboxylate ($-COO^-$) and carbonyl [$-(C{=}O)^-$] termini and positively charged $-NH_3^+$ termini in OPN are responsible for strong binding interactions with HAP and OC. These termini can form bonds with calcium in HAP and NH_3^+ termini in OC. Moreover, amino termini of OPN can form bonds within the carboxyl terminal of OC.[18,43−46] More detail about the OPN and OC chains is given in Table S1.

System Assembly. To investigate the biomechanics of the collagen interfibrillar interface at the nanoscale, first, the atomistic models of noncollagenous OC/OPN protein complexes were established and were placed between two HAP mineral platelets as shown in Figure 1B. The length and width of the HAP platelets were assumed to be 32.1 and 22.3 nm with the thickness of 2.4 nm.[47−49] The reported value for the nano-interface thickness in the literature[50,51] is close to the value obtained in the present study 2.6 nm (the initial gap between HAP platelets). Based on the experimental results reported in ref 16, the mole ratio of OC to OPN in the bone was assumed to be 16:1. More details on the mole and mass ratio are discussed in the Supporting Information. Three parallel layers of protein chains filled the gap between two HAP platelets. The top and bottom layers both consisted of 32 OCs evenly distributed on the HAP surface because OC is known to bind far more strongly to mineral than OPN. Furthermore, a middle layer of OPN between two OC layers is considered (the side-view in Figure 1B) because OPN is found predominantly in the dilatational band regions.[16,52] The middle layer had four OPNs evenly scattered in the gap between the OC layers, and OPNs do not have a direct contact with HAP platelets. Different placement of proteins may affect deformation mechanisms and alter the dissipated energy in the nano-interface.

The model was placed in the center of a 100 nm cubic box. 1000 water molecules were added to the system, and periodic boundary conditions in x, y, z directions were applied. Ca^{2+} ions were also added to neutralize the system. Strong electrostatic interactions between Ca^{2+} ions and oxygen atoms of ASP and GLU residues in proteins and PO_4^{3-} and OH^- ions in HAP can be formed. Therefore, calcium ions function as bridges and allow proteins to attach to the HAP surface. The charge and geometrical properties of the model are given in Table S2.

Molecular Dynamic Simulation. MD simulations were carried out in GROMACS 5.1.2 package using the CHARMM36 force field.[53] After the system assembly, the energy of the system was minimized using the steepest descent algorithm. Steered MD was used for the simulations. Initially, the protein assembly was pressed by two HAP platelets under external pressing force. Then, the pressing force was released, and the HAPs were allowed to freely move back to get the protein chains relaxed. In this relaxation step, the system was equilibrated for 2 nanoseconds at the *NVT* ensemble at a temperature of 310 K until the final model was obtained. After that, different loadings were applied to the HAP platelets to investigate the mechanical response of the nano-interface. The mass centers of HAP platelets were attached to a spring and forced to move along the tangent and normal directions, for shear and tension deformations, respectively. A pulling velocity of 2 pm/ps was used for all loading conditions. The force and displacements were then recorded and used for stress and strain calculations. Each simulation was run three times to obtain statistical data.

Calculation of Stress, Strain, and Specific Energy. The interface in bone is subjected to different loadings, that is, shear, tension, and compression (Figure 1A). The engineering stress and strain for each loading conditions were obtained by considering the height and cross-sectional area of the interface and the displacement of HAP platelets (Figure 1D). The stress and strain were defined as $\tau = F_S/A_0$ and $\gamma = 2d/h$ in shear, and $\sigma = F_T/A_0$ and $\varepsilon = \Delta/h$ in tension, respectively. τ and γ are shear stress and shear strain, respectively; σ and ε are normal stress and normal strain; and $\Delta = H - h$. As it is shown in Figure 1D, h and H are the distances between HAP platelets in the initial and current configurations, respectively. A_0 and d are the initial in-plane cross-sectional area of the protein interface and the displacement of HAP platelets in the Y-direction as depicted in Figure 1D. The values of A_0 and h are given in Table S2. The ultimate strength was defined as the maximum stress that the interface can withstand. The specific energy was obtained by the area under the stress−strain curve divided by the mass of the nano-interface. It is worth mentioning that ∼92% of the interface weight is from the HAP platelets. Therefore, excluding the weight of the HAP platelets would result in more than 10 times increase in the specific energy reported here.

Bond Energy and Gyration Radius. The bond energy is composed of bond stretch, bond angle, and dihedral energy. Gyration radius (R_g) is another important parameter that provides quantitative information for the configuration change. The R_g of a protein is a measure of its compactness. If a protein is stably folded, it will likely

DOI: 10.1021/acsbiomaterials.9b00588
ACS Biomater. Sci. Eng. 2019, 5, 5916−5924

maintain a relatively steady value of R_g. If a protein unfolds or stretches, its R_g will change.

Interaction Energy. Interaction energy is the energy between noncovalent atoms and is the summation of electrostatic and van der Waals interactions. The negative value for interaction energy means attractive interaction. To obtain the number of bonds that form and break during deformation, we calculated the number of noncovalently bonded pairs. Here, we counted the number of interaction pairs within the cut-off distance of 3.5 Å. The number of bonds was used to find the change in the interaction and configuration of the chains.

■ ASSOCIATED CONTENT

Supporting Information

The Supporting Information is available free of charge on the ACS Publications website at DOI: 10.1021/acsbiomaterials.9b00588.

Mechanical properties of the nano-interface; interaction energies; binding sites; variations in bond energies; and theoretical staggered model (PDF)

■ AUTHOR INFORMATION

Corresponding Author

*E-mail: majid.minary@utdallas.edu.

ORCID

Majid Minary-Jolandan: 0000-0003-2472-302X

Author Contributions

M.M.-J. and D.Q. designed the research and provided the guidelines. R.M., Z.D., and Y.W. executed the research. All the authors contributed to manuscript writing.

Notes

The authors declare no competing financial interest.

■ ACKNOWLEDGMENTS

This work was supported by the grant from the US National Science Foundation (award CMMI-1727960), the US Air Force Office of Scientific Research (FA9550-14-1-0252), and the National Natural Science Foundation of China (grant no. 51303065). The authors appreciate the discussion of the research with Dr. Zhong Zhou.

■ REFERENCES

(1) Zimmermann, E. A.; Ritchie, R. O. Bone as a Structural Material. *Adv. Healthcare Mater.* **2015**, *4*, 1287−1304.

(2) Zimmermann, E. A.; Busse, B.; Ritchie, R. O. The fracture mechanics of human bone: influence of disease and treatment. *BoneKEy Rep.* **2015**, *4*, 743 DOI: 10.1038/Bonekey.2015.112.

(3) Koester, K. J.; Ager, J. W.; Ritchie, R. O. The true toughness of human cortical bone measured with realistically short cracks. *Nat. Mater.* **2008**, *7*, 672−677.

(4) Barthelat, F.; Yin, Z.; Buehler, M. J. Structure and mechanics of interfaces in biological materials. *Nat. Rev. Mater.* **2016**, *1*, 16007.

(5) Wang, R.; Gupta, H. S. Deformation and Fracture Mechanisms of Bone and Nacre. *Annu. Rev. Mater. Res.* **2011**, *41*, 41−73.

(6) Ritchie, R. O. The conflicts between strength and toughness. *Nat. Mater.* **2011**, *10*, 817−822.

(7) Minary-Jolandan, M.; Yu, M.-F. Nanomechanical Heterogeneity in the Gap and Overlap Regions of Type I Collagen Fibrils with Implications for Bone Heterogeneity. *Biomacromolecules* **2009**, *10*, 2565−2570.

(8) Minary-Jolandan, M.; Yu, M.-F. Uncovering Nanoscale Electromechanical Heterogeneity in the Subfibrillar Structure of Collagen Fibrils Responsible for the Piezoelectricity of Bone. *ACS Nano* **2009**, *3*, 1859−1863.

(9) Smith, B. L.; Schäffer, T. E.; Viani, M.; Thompson, J. B.; Frederick, N. A.; Kindt, J.; Belcher, A.; Stucky, G. D.; Morse, D. E.; Hansma, P. K. Molecular mechanistic origin of the toughness of natural adhesives, fibres and composites. *Nature* **1999**, *399*, 761−763.

(10) Thurner, P. J.; Chen, C. G.; Ionova-Martin, S.; Sun, L.; Harman, A.; Porter, A.; Ager, J. W.; Ritchie, R. O.; Alliston, T. Osteopontin deficiency increases bone fragility but preserves bone mass. *Bone* **2010**, *46*, 1564−1573.

(11) Thompson, J. B.; Kindt, J. H.; Drake, B.; Hansma, H. G.; Morse, D. E.; Hansma, P. K. Bone indentation recovery time correlates with bond reforming time. *Nature* **2001**, *414*, 773−776.

(12) Gupta, H. S.; Fratzl, P.; Kerschnitzki, M.; Benecke, G.; Wagermaier, W.; Kirchner, H. O. K. Evidence for an elementary process in bone plasticity with an activation enthalpy of 1 eV. *J. R. Soc., Interface* **2007**, *4*, 277−282.

(13) Fantner, G. E.; Adams, J.; Turner, P.; Thurner, P. J.; Fisher, L. W.; Hansma, P. K. Nanoscale ion mediated networks in bone: Osteopontin can repeatedly dissipate large amounts of energy. *Nano Lett.* **2007**, *7*, 2491−2498.

(14) Hansma, P. K.; Fantner, G. E.; Kindt, J. H.; Thurner, P. J.; Schitter, G.; Turner, P. J.; Udwin, S. F.; Finch, M. M. Sacrificial bonds in the interfibrillar matrix of bone. *J. Musculoskeletal Neuronal Interact.* **2005**, *5*, 313−315.

(15) Fantner, G. E.; Hassenkam, T.; Kindt, J. H.; Weaver, J. C.; Birkedal, H.; Pechenik, L.; Cutroni, J. A.; Cidade, G. A. G.; Stucky, G. D.; Morse, D. E.; Hansma, P. K. Sacrificial bonds and hidden length dissipate energy as mineralized fibrils separate during bone fracture. *Nat. Mater.* **2005**, *4*, 612−616.

(16) Poundarik, A. A.; Diab, T.; Sroga, G. E.; Ural, A.; Boskey, A. L.; Gundberg, C. M.; Vashishth, D. Dilatational band formation in bone. *Proc. Natl. Acad. Sci.* **2012**, *109*, 19178−19183.

(17) Gupta, H. S.; Wagermaier, W.; Zickler, G. A.; Raz-Ben Aroush, D.; Funari, S. S.; Roschger, P.; Wagner, H. D.; Fratzl, P. Nanoscale deformation mechanisms in bone. *Nano Lett.* **2005**, *5*, 2108−2111.

(18) Zhou, Z.; Qian, D.; Minary-Jolandan, M. Clustering of hydroxyapatite on a super-twisted collagen microfibril under mechanical tension. *J. Mater. Chem. B* **2017**, *5*, 2235−2244.

(19) Zhou, Z.; Minary-Jolandan, M.; Qian, D. A simulation study on the significant nanomechanical heterogeneous properties of collagen. *Biomech. Model. Mechanobiol.* **2015**, *14*, 445−457.

(20) Ritchie, R. O. The conflicts between strength and toughness. *Nat. Mater.* **2011**, *10*, 817.

(21) Zioupos, P.; Kaffy, C.; Currey, J. D. Tissue heterogeneity, composite architecture and fractal dimension effects in the fracture of ageing human bone. *Int. J. Fract.* **2006**, *139*, 407−424.

(22) Braidotti, P.; Bemporad, E.; D'Alessio, T.; Sciuto, S. A.; Stagni, L. Tensile experiments and SEM fractography on bovine subchondral bone. *J. Biomech.* **2000**, *33*, 1153−1157.

(23) Ritchie, R. O.; Buehler, M. J.; Hansma, P. Plasticity and toughness in bone. *Phys. Today* **2009**, *62*, 41−47.

(24) Hang, F.; Gupta, H. S.; Barber, A. H. Nanointerfacial strength between non-collagenous protein and collagen fibrils in antler bone. *J. R. Soc., Interface* **2014**, *11*, 20130993.

(25) Hang, F.; Barber, A. H. Nano-mechanical properties of individual mineralized collagen fibrils from bone tissue. *J. R. Soc., Interface* **2010**, *8*, 500−505.

(26) Steiglitz, B. M.; Kreider, J. M.; Frankenburg, E. P.; Pappano, W. N.; Hoffman, G. G.; Meganck, J. A.; Liang, X.; Hook, M.; Birk, D. E.; Goldstein, S. A.; Greenspan, D. S. Procollagen C Proteinase Enhancer 1 Genes Are Important Determinants of the Mechanical Properties and Geometry of Bone and the Ultrastructure of Connective Tissues. *Mol. Cell. Biol.* **2006**, *26*, 238.

(27) Wang, C.-a.; Huang, Y.; Zan, Q.; Guo, H.; Cai, S. Biomimetic structure design—a possible approach to change the brittleness of ceramics in nature. *Mater. Sci. Eng. C* **2000**, *11*, 9−12.

(28) Rath, J. P.; Chaki, T. K.; Khastgir, D. Change in fiber properties due to the heat treatment of nylon 6 tire cords. *J. Appl. Polym. Sci.* **2008**, *108*, 3960−3967.

DOI: 10.1021/acsbiomaterials.9b00588
ACS Biomater. Sci. Eng. 2019, 5, 5916−5924

(29) Motta, M.; Moisala, A.; Kinloch, I. A.; Windle, A. H. High performance fibres from "dog bone"carbon nanotubes. *Adv. Mater.* **2007**, *19*, 3721−3726.
(30) Miaudet, P.; Badaire, S.; Maugey, M.; Derré, A.; Pichot, V.; Launois, P.; Poulin, P.; Zakri, C. Hot-drawing of single and multiwall carbon nanotube fibers for high toughness and alignment. *Nano Lett.* **2005**, *5*, 2212−2215.
(31) Vollrath, F.; Knight, D. P. Liquid crystalline spinning of spider silk. *Nature* **2001**, *410*, 541.
(32) Zhang, M.; Atkinson, K. R.; Baughman, R. H. Multifunctional carbon nanotube yarns by downsizing an ancient technology. *Science* **2004**, *306*, 1358−1361.
(33) Naraghi, M.; Filleter, T.; Moravsky, A.; Locascio, M.; Loutfy, R. O.; Espinosa, H. D. A multiscale study of high performance double-walled nanotube− polymer fibers. *ACS Nano* **2010**, *4*, 6463−6476.
(34) Porter, D.; Vollrath, F.; Shao, Z. Predicting the mechanical properties of spider silk as a model nanostructured polymer. *Eur. Phys. J. E* **2005**, *16*, 199−206.
(35) Gosline, J.; Guerette, P.; Ortlepp, C.; Savage, K. The mechanical design of spider silks: from fibroin sequence to mechanical function. *J. Exp. Biol.* **1999**, *202*, 3295−3303.
(36) Wood, L. A.; Bekkedahl, N.; Roth, F. L. Density measurements on synthetic rubbers. *Rubber Chem. Technol.* **1943**, *16*, 244−248.
(37) Papkov, D.; Zou, Y.; Andalib, M. N.; Goponenko, A.; Cheng, S. Z. D.; Dzenis, Y. A. Simultaneously strong and tough ultrafine continuous nanofibers. *ACS Nano* **2013**, *7*, 3324−3331.
(38) Cai, J.; Naraghi, M. Non-intertwined graphitic domains in nanoscale leads to super strong and tough continuous 1D nanostructures. *Carbon* **2018**, *137*, 242−251.
(39) Frazão, C.; Simes, D. C.; Coelho, R.; Alves, D.; Williamson, M. K.; Price, P. A.; Cancela, M. L.; Carrondo, M. A. Structural evidence of a fourth Gla residue in fish osteocalcin: biological implications. *Biochemistry* **2005**, *44*, 1234−1242.
(40) Agarwala, R.; Barrett, T.; Beck, J.; Benson, D. A.; Bollin, C.; Bolton, E.; Bourexis, D.; Brister, J. R.; Bryant, S. H.; Canese, K. Database resources of the national center for biotechnology information. *Nucleic Acids Res.* **2018**, *46*, D8−D13.
(41) Lin, T.-J. Force Field Parameters and Atomistic Surface Models for Hydroxyapatite and Analysis of Biomolecular Adsorption at Aqueous Interfaces. Ph.D. Thesis, The University of Akron, Akron, Ohio, 2013, p 131.
(42) Wilson, R. M.; Elliott, J. C.; Dowker, S. E. P. Rietveld refinement of the crystallographic structure of human dental enamel apatites. *Am. Mineral.* **1999**, *84*, 1406−1414.
(43) Lai, Z. B.; Wang, M.; Yan, C.; Oloyede, A. Molecular dynamics simulation of mechanical behavior of osteopontin-hydroxyapatite interfaces. *J. Mech. Behav. Biomed. Mater.* **2014**, *36*, 12−20.
(44) Addison, W. N.; Masica, D. L.; Gray, J. J.; McKee, M. D. Phosphorylation-dependent inhibition of mineralization by osteopontin ASARM peptides is regulated by PHEX cleavage. *J. Bone Miner. Res.* **2010**, *25*, 695−705.
(45) Kaartinen, M. T.; Pirhonen, A.; Linnala-Kankkunen, A.; Mäenpää, P. H. Transglutaminase-catalyzed cross-linking of osteopontin is inhibited by osteocalcin. *J. Biol. Chem.* **1997**, *272*, 22736−22741.
(46) Bolander, M. E.; Young, M. F.; Fisher, L. W.; Yamada, Y.; Termine, J. D. Osteonectin cDNA sequence reveals potential binding regions for calcium and hydroxyapatite and shows homologies with both a basement membrane protein (SPARC) and a serine proteinase inhibitor (ovomucoid). *Proc. Natl. Acad. Sci.* **1988**, *85*, 2919−2923.
(47) Burger, C.; Zhou, H.-w.; Wang, H.; Sics, I.; Hsiao, B. S.; Chu, B.; Graham, L.; Glimcher, M. J. Lateral Packing of Mineral Crystals in Bone Collagen Fibrils. *Biophys. J.* **2008**, *95*, 1985−1992.
(48) Launey, M. E.; Buehler, M. J.; Ritchie, R. O. On the Mechanistic Origins of Toughness in Bone. *Annu. Rev. Mater. Res.* **2010**, *40*, 25−53.
(49) Fratzl, P.; Fratzl-Zelman, N.; Klaushofer, K.; Vogl, G.; Koller, K. Nucleation and growth of mineral crystals in bone studied by small-angle X-ray scattering. *Calcif. Tissue Int.* **1991**, *48*, 407−413.
(50) Hang, F.; Gupta, H. S.; Barber, A. H. Nanointerfacial strength between non-collagenous protein and collagen fibrils in antler bone. *J. R. Soc., Interface* **2014**, *11*, 20130993.
(51) Fratzl, P.; Weinkamer, R. Nature's hierarchical materials. *Prog. Mater. Sci.* **2007**, *52*, 1263−1334.
(52) Fantner, G. E.; Hassenkam, T.; Kindt, J. H.; Weaver, J. C.; Birkedal, H.; Pechenik, L.; Cutroni, J. A.; Cidade, G. A. G.; Stucky, G. D.; Morse, D. E.; Hansma, P. K. Sacrificial bonds and hidden length dissipate energy as mineralized fibrils separate during bone fracture. *Nat. Mater.* **2005**, *4*, 612.
(53) Berendsen, H. J. C.; van der Spoel, D.; van Drunen, R. GROMACS: A message-passing parallel molecular dynamics implementation. *Comput. Phys. Commun.* **1995**, *91*, 43−56.

NOTE ADDED AFTER ASAP PUBLICATION

This paper was published ASAP on October 9, 2019 with an incorrect Figure 4. The corrected version was reposted on October 10, 2019.

DOI: 10.1021/acsbiomaterials.9b00588
ACS Biomater. Sci. Eng. 2019, 5, 5916−5924